



# High velocity oxy-fuel (HVOF) sprayed coating nanoarchitectonics: influence of reduced graphene oxide (rGO) on tribological characteristics

Akella Srikanth<sup>1</sup> · Venkateshwarlu Bolleddu<sup>1</sup>

Received: 13 November 2022 / Accepted: 25 March 2023 / Published online: 4 April 2023  
© The Author(s), under exclusive licence to Springer-Verlag GmbH, DE part of Springer Nature 2023

## Abstract

In thermally sprayed tungsten carbide–cobalt (WC–Co) coatings, the hard WC particles perform as the wear-resistant part, while the cobalt act as binder and provides toughness. Due to their excellent properties, thermally sprayed WC–Co coatings have been widely used in many industrial applications requiring sliding, abrasion, erosion resistance, and fretting. The Tribological characteristics of nanostructured WC-25%Co coatings obtained using high velocity oxy-fuel (HVOF) spraying were investigated. The feedstock powder of nanostructured WC-25%Co used to deposit the coatings was mixed with the reduced graphene oxide (rGO) as an additive at three different weight percentages proportions of 0.5, 1.0, and 1.5 wt% to investigate its effect on the characteristics of coatings. The microstructural and tribological characteristics of obtained coatings were evaluated. The worn-out surfaces of coatings in the wear track were characterized to identify the wear mechanism involved. It is found that abrasion wear is the most predominant wear mechanism causing the wear loss of coatings. It is also found from wear track analysis that wear tracks are evident at 1.5 and 1.0 kgf loading conditions, while they are very lightly visible at 0.5 kgf loading condition because of lesser impact of WC ball over the coating surface. Microstructural characteristics of the coatings are altered, and the rGO bridges in the middle of the splats are also identified in coating's microstructure. Also, a significant improvement is observed in the microhardness and surface roughness with rGOs reinforcement in the nanostructured coatings.

**Keywords** WC–Co coatings · Nanostructured coatings · HVOF spraying · Reduced graphene oxide · Tribological characteristics

## 1 Introduction

The damage of component materials in engineering systems are happened as a result of wear is very undesirable and leads to repair or replacement of components which otherwise results in their failure. Numerous works are done to study and understand the mechanisms of wear and also to develop the wear characteristics of the materials. It is understood that the surface modification using hard thick protective coatings on metallic substrates of components can certainly increase the wear resistance. Thus, surface

engineering takes part an important role in wear reduction and in addition to corrosion-induced damage of components used in various industries [1, 2]. Also, material deprivation in service span of components in the thermal environment is not just troublemaking but also not advisable to the economy of production.

To conquer all these problems, researchers have built up a protective shield for covering the material of engineering applications with viable coatings obtained from ceramic feedstock powders. It will enhance the material lifetime, while the coating is demonstrated to be resistant to wear damages and mechanically strong [3]. Different investigations have been performed on ceramic type of coatings to determine microstructural, mechanical and wear properties on the surface of material. These examinations proved that the wear resistance is significantly influenced by various properties, such as powder grain size, hardness, phase distribution, binder phase content, microstructure, and also

✉ Venkateshwarlu Bolleddu  
venkateshwarlu.b@vit.ac.in; venkatsoft2004@gmail.com

<sup>1</sup> Department of Manufacturing, School of Mechanical Engineering, Vellore Institute of Technology, Vellore 632014, India

toughness of the coating material [4]. However, due to their superior properties the ceramic materials are widely used in various industrial applications. The main reason for using ceramic coatings is to get resistance from wear to attain higher hardness. [5–7].

In recent times, depositions of ceramic coatings on the surface of metallic substrates are performed through different types of deposition methods. Among these high velocity oxy-fuel (HVOF) is one of the most prominent techniques for deposition of coatings under elevated environments and temperatures. Nowadays, thermal barrier coatings (TBC) are used significantly in aviation industries to get protection from erosion, wear, pores and other defects. [8]. HVOF thermal barrier coatings are mainly utilized in heat engines at elevated temperatures to get resistance from wear. During spraying, these composite powders are heated up to 3000 K and accelerated at higher velocity in a chemically active environment [9].

Tungsten carbide–cobalt (WC–Co) coatings are known for wear resistant coatings due to their excellent sliding wear resistance and mechanical properties. The coatings should resist the wear and corrosion, while material undergoes at extreme temperatures. The main features that influence the performance of TBCs are pores, which are located in coatings microstructure. Therefore, numerous experiments are conducted to recognize the relationship between microstructure, porosity, processing methods, and the properties including thermal shock resistance, heat conductivity, fracture toughness, micro hardness, etc. [10, 11].

Reduced graphene oxide (rGO) is one of the best alternatives to improve the wear resistance and very few studies have been conducted to investigate the characteristics of the coatings obtained from rGO doped ceramic feedstock powder. Graphene is a formation of single layer carbon atoms possessing 2D-hexagonal structure and it has been attracted widely in major industrial applications due to its unique features [12–15]. Graphene is not only the thinnest material but also it can exhibit the highest thermal conductivity possess above  $3000 \text{ W m}^{-1} \text{ K}^{-1}$ , and electrical conductivity of  $2.5 \times 10^5 \text{ cm}^2 \text{ V}^{-1} \text{ s}^{-1}$  [16], greater mechanical properties of 1 TPa Young's modulus, and 130 GPa intrinsic strength [17–19]. However, using graphene alone for the coatings on metallic substrates is very difficult due to its single layer formation and hence it cannot protect the surface completely. Schriver et al. [20] obtained the graphene reinforced Cu metal coatings using chemical vapor deposition (CVD) process. It is observed that there are many defects on coating surface and it has undergone severe oxidation process. A possible solution defined to prevent these kinds of issues is using graphene based oxides like reduced graphene oxide [21, 22]. The rGO is a purified form of GO obtained from reduction of oxygen-related functional groups of graphene oxide through thermal or chemical techniques.

In this study, HVOF sprayed nanostructured coatings obtained from rGO added WC-25wt.%Co feedstock powder were characterized to investigate the powder morphology, coating microstructure, phase analysis, surface roughness, and also the tribological characteristics, such as the weight loss against normal load, average coefficient of friction, wear track morphology, and the wear mechanisms involved.

## 2 Experimental procedures

In this work, the high velocity oxy-fuel (HVOF) spraying process was used for the deposition of coatings. The coatings were deposited by utilizing a spraying gun (DJ 2600 model) having a nozzle (DJ 2603 model) at *Spraymet Surface Technologies Private Limited, Bangalore, India*. The nanostructured WC-25 wt% Co feedstock powder was reinforced with reduced graphene oxide to obtain the corresponding coatings. The feedstock powders with an average particle size of 30–50 nm were added with the reduced graphene oxide (rGO) at three different percentage proportions of 0.5, 1, and 1.5 wt%. The feedstock powders of WC-25 wt% Co, and rGO were obtained from *Nano Research Lab, Jamshedpur, Jharkhand, India*. It can be noted that the nanostructured WC-25 wt% Co powders were mixed properly with rGO having an average particle size of 20–45  $\mu\text{m}$  using ball milling process (at 180 rpm for 1 h) at three different percentage proportions of 0.5, 1, and 1.5 wt%. As per the information from the powder's supplier, the tap densities of nanostructured WC-25 wt% Co and rGO are  $3.9 \text{ g/cm}^3$ , and  $1.91 \text{ g/cm}^3$ , respectively. The schematic representation of HVOF coating and characterization studies are shown in Fig. 1. The process parameters used for HVOF spraying of coatings are shown in Table 1.

### 2.1 Sample preparation and coatings deposition

The mild steel (AISI 1020) substrates ( $100 \times 100 \times 6 \text{ mm}$ ) were used for the coatings deposition. First, to remove unwanted oxides from surface, the substrates were ground using a surface grinder (Alex NH 500 model) and an average surface roughness of  $0.1 \mu\text{m}$  was maintained on the substrate surface. For better mechanical anchor and adhesion during coatings deposition, the substrates were grit blasted with an alumina grits having an average grit size of 28 and at 140 psi air pressure. After grit blasting, to remove the dust, dirt, and any other foreign particles completely, the substrates were ultrasonically cleaned in an iso-propanol bath for 15–20 min. Later, the substrates were fixed on the substrate holder and pre-heated to a temperature of around  $100\text{--}150 \text{ }^\circ\text{C}$ , and then the nanostructured WC-25 wt% Co coatings reinforced with rGO were deposited using HVOF spraying. The thickness of the coating was ranging from

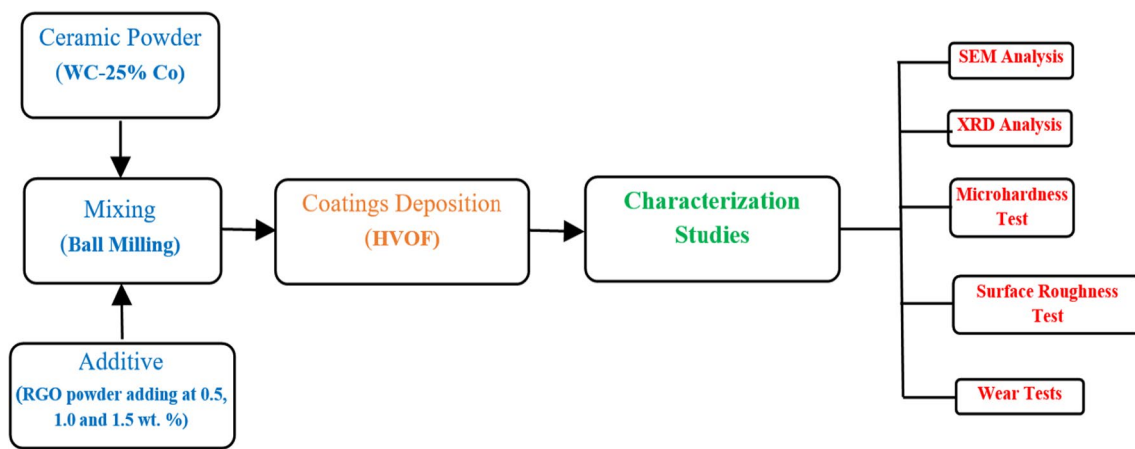


**Fig. 1** Schematic representation of high velocity oxy-fuel (HVOF) sprayed rGO induced WC-25%Co coatings

**Table 1** Process parameters used for HVOF spraying process

| Parameter                                  | Range           |
|--|-----------------|
| Flow rate of Oxygen (O <sub>2</sub> )      | 1000–1050 l/min |
| Flow rate of Kerosene                      | 0.45 l/min      |
| Flow rate of carrier gas (H <sub>2</sub> ) | 60–70 l/min     |
| Powder feed rate                           | 80–100 g/min    |
| Spray velocity                             | 1200 m/s        |
| Spray distance                             | 205–260 mm      |

300 to 350  $\mu\text{m}$ . For further investigation to study the coating characteristics and properties, the coated samples were cut into cross-sectional specimens of size  $10 \times 5 \times 6$  mm using a low speed diamond saw cutter. Later, these cross-sectional specimens were hot mounted using Bakelite powder for metallographic studies. These hot mounted specimens were polished with SiC abrasive sheets of different grades 220, 400, 600, 800, and 1000. Polishing was done on each abrasive paper for 10 min and later disc polishing on velvet cloth was also carried out for 15 min.

## 2.2 Characterization and analysis

The coatings microstructure on cross-sectional specimens was examined using Zeiss EVO 18 scanning electron microscope (SEM). For each coating variant, seven images were taken at various magnifications. To study the phases, present in the powder and coatings, X-ray diffraction (XRD) tests were performed using X-ray diffractometer (PANalytical X'pert PRO PW1070) with CuK $\alpha$  radiation, 40 kV operating voltage, 40 mA current, step time of 0.14 s, and scanning step of 0.0172°.

Measurement of microhardness on the cross section of coatings was performed using microhardness tester (MMT\_X7B model) with Vicker's microhardness indenter at load

**Table 2** Parameters used in wear tests

| Parameter        | Value               |
|------------------|---------------------|
| Load             | 0.5, 1.0, 1.5 kgf   |
| Sliding distance | 300 m               |
| Sliding speed    | 0.17, 0.33, 0.5 m/s |
| Track diameter   | 10 mm               |

of 100 g and dwell time of 15 s. Average of ten readings was computed for each type of coating sample. The surface roughness measurement of as-sprayed coatings was also carried out using a profilometer (Marsurf precision model) integrated with Taly Profile software at chosen ten random locations, and average surface roughness (Ra) was calculated.

## 2.3 Tribological study

Numerous wear tests were carried out on coating sample surface by Ducom tribometer (model: TR-20-OLE) to observe the wear depth, coefficient of friction (COF), wear depth, and the wear rate. The parameters employed for performing wear tests are mentioned in Table 2. These tests were carried out at various types of loads of 0.5, 1.0, and 1.5 kgf and maintain sliding speeds of 0.17, 0.33, and 0.5 m/s. The sliding distance was set as constant at 300 m. The WC (tungsten carbide) balls were utilized for these wear tests with a diameter of 8 mm. The weight loss of the as-sprayed coated samples was calculated using Essae company model: FB-600 electronic balance by determining the coated sample weight before and after performing the wear test. After finishing each wear test the wear debris over the sample was removed completely by air blowing process. The wear tests were conducted at each loading condition by maintain with three different speed conditions to get the accurate results. Total three different loads were used to check the wear

behavior of coated sample at three different speeds of each load. The standard deviation and mean for the sample weight loss were calculated. Finally, after wear test the wear tracks morphology were examined with SEM analysis to observe the mechanisms included in wear track. The wear rate was calculated using the below mentioned equation:

$$Wr = V/F \cdot L, \quad (1)$$

where  $Wr$  is the wear rate ( $\text{mm}^3/\text{Nm}$ ),  $V$  is the wear volume ( $\text{mm}^3$ ),  $F$  is the normal load (N), and  $L$  is the sliding distance (m).

The wear volume ( $V$ ) is computed with below stated equation:

$$V = (W_0 - W)/D, \quad (2)$$

where  $W_0$  is the weight of sample before performing test,  $W$  is the weight of the sample after performing test, and  $D$  is the powder density.

The density of tungsten carbide–cobalt powder is  $3.64 \text{ g}/\text{cm}^3$

(Data acquired from the powder supplier Nano research Lab, Jamshedpur, India).

### 3 Results and discussion

#### 3.1 Microstructure and phase analysis

To study the powder morphology and microstructure of coatings the SEM analysis is carried out. The feedstock powder morphology of nanostructured WC-25 wt% Co before and after addition of rGO is shown in Figs. 2 and 3. It could be seen from Fig. 1 that the nanostructured WC-25 wt% Co feedstock powders before the addition of rGO are spherical in shape and having more pores. It is known that high energy ball milling is a simple and efficient way of manufacturing the fine powder with nanostructure size. Powder mixture of

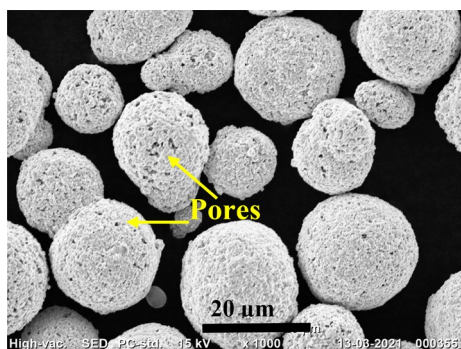


**Fig. 2** Powder morphology of WC-25 wt% Co powder before adding rGO

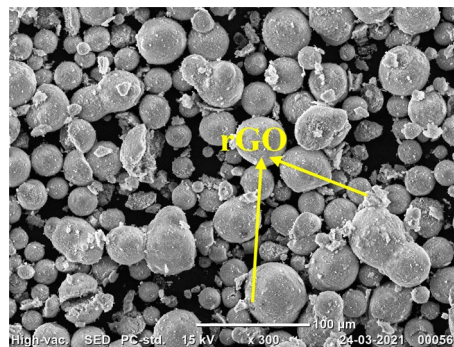


**Fig. 3** Powder morphology of WC-25 wt% Co powder after adding rGO

WC-25 wt% Co were closed up in WC–Co hard metal vial mixed with ethanol and WC–Co hard metal balls of 8 and 12 mm in diameter is used for mixing in a glove box containing inert atmosphere of Ar. The ball to powder weight ratio is controlled to be 15:1. The milling process was continued on a high energy ball mill with the selected rotation velocity of 250 rpm. After 10 h duration of milling, the powder was taken out from vial and dried it up at room temperature [23]. The spherical morphology assists in powder better flow at the time of deposition of coatings. The pores can be seen clearly at higher zoom level and the outer surface of powder particles look very rough. The pores are appearing as black in the SEM micrograph. Nanostructured powders with hollow and porous morphology have higher surface area being exposed to gas and, thereby, the WC phase in the powders is expected to undergo greater decomposition and dissolution as compared to conventional powders [24]. Morphology of the powder after the addition of the rGOs is revealed in Fig. 3 and the adherence of rGOs over WC and cobalt powder particles can be seen clearly in the powders added with 1.5 wt% rGO. It can also be identified that the rGO dispersed uniformly in the powder and lowered the amount of pores resulting in reduced porosity [25, 26].

The coating process of rGO reinforced WC-25 wt% Co powder is shown illustratively in Fig. 4. Cross-sectional micrograph showing the microstructure of WC-25 wt% Co coatings obtained from feedstock powders before addition of rGO is shown in Fig. 5. It could be observed from Fig. 5 that the WC-25 wt% Co coating exhibiting many pores in its microstructure and the pores are visible as tiny dark areas. Greater densities of finer and uniformly distributed WC particles are identified (see Fig. 5) in HVOF sprayed coatings.

The microstructure of WC-25 wt% Co coatings obtained from feedstock powders after the addition of rGOs is revealed in Fig. 6. It could be observed that the rGOs have stickled and well dispersed in the microstructure of coating sample [27]. It can also be identified that the reinforcement of 1.5 wt% rGOs in these nanostructured coatings caused



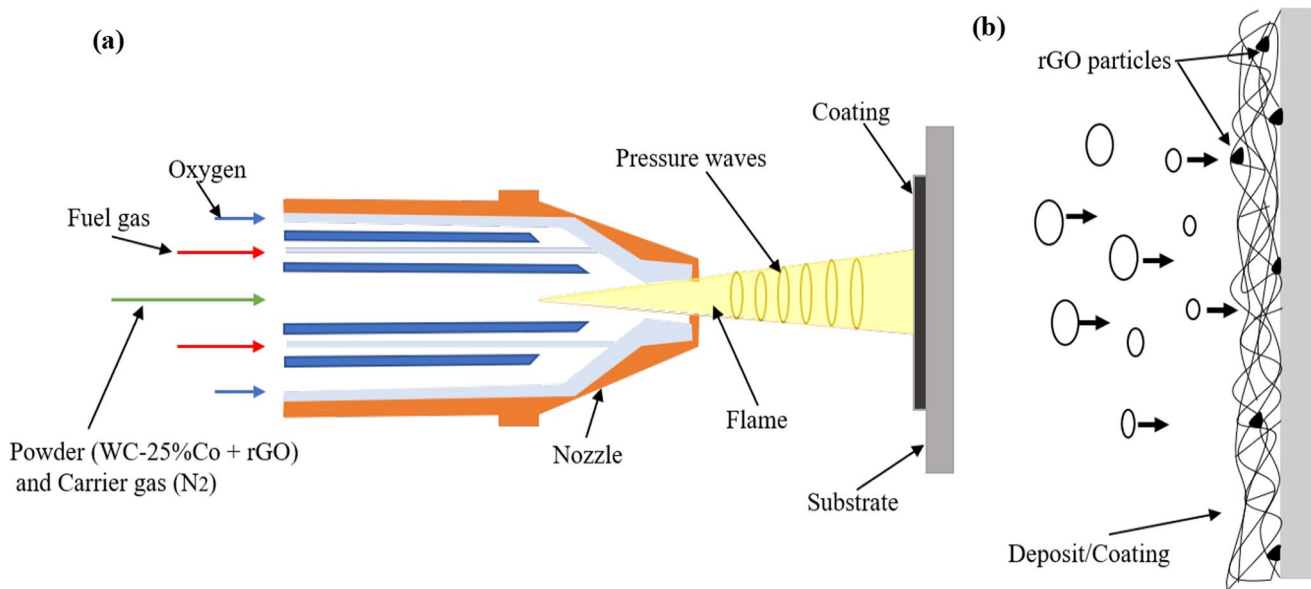


**Fig. 4** Illustrative representation of **a** high velocity oxy-fuel (HVOF) coating process; **b** powder particles coated on the substrate

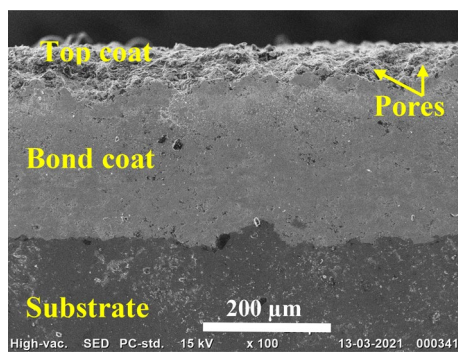


**Fig. 5** Cross-sectional microstructure of WC-25%Co without rGO addition

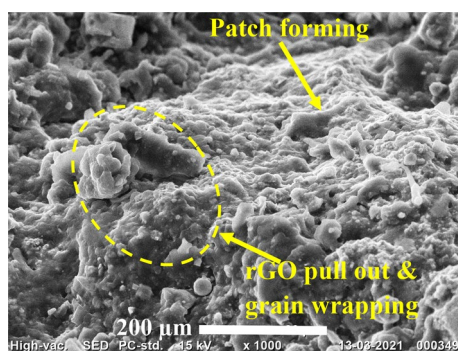


**Fig. 6** Topcoat cross-sectional microstructure of WC-25 wt% Co coatings after addition of 1.5 wt% rGO

for the formation of patches in the microstructure and this is accredited to decarbonization of the coatings at elevated temperatures at the time of coatings deposition. The microstructure also contains multiple micro pits with wavy nature. The surface also seems to be very rough. The rGO pullout also can be seen in Fig. 6 that requires the dissipation of more fracture energy as it is having higher interfacial area on the external force application. Therefore, the toughness increases automatically which can delay the fracture of the coatings. The results are in line with the work carried out by Neito et al. [28], and it was observed that the increased fracture toughness of coatings is due to both graphene nanoparticles sliding and bending. Figure 6 also displays the grain wrapping by rGO, which can oppose the crack initiation efficiently by holding the grain jointly in the partially melted regions and re-solidified area [29]. The same observation of graphene nanoparticles grain wrapping with alumina coatings in the plasma sprayed coatings was identified by Mukherjee et al. [30]

The phases present in powders and the coatings before and after the addition of rGOs have been investigated. Tungsten carbide (WC), and cobalt (Co) were only the major phases located in WC-25 wt% Co powder before adding rGO and it is shown in Fig. 7. It can be seen that the intensity of cobalt phase is less as compared to the tungsten carbide phase because of its lesser percentage in the powder composition. However, an additional phase of carbon (C) was also identified after the addition of rGOs. However, this phase is neglected and not displayed here as a result of its very less intensity.

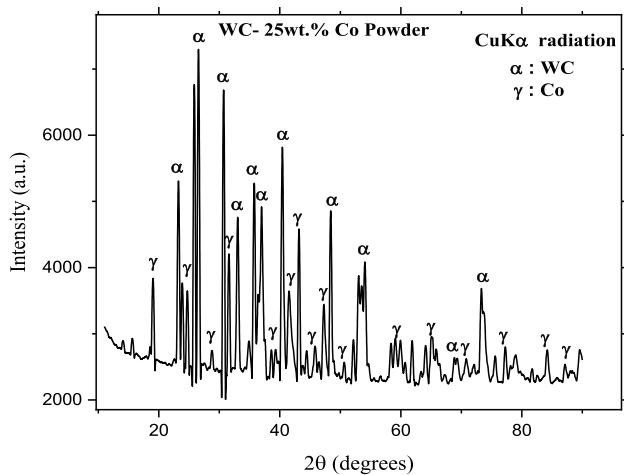


**Fig. 7** Phase analysis of WC-25 wt% Co powder without rGO

Correspondingly, the phases present in WC-25 wt% Co coatings before and after rGOs addition are displayed in Fig. 8. It could be identified from Fig. 8a that the coatings obtained without rGO addition contain the phases of tungsten (W), tungsten carbide (WC), and semi-tungsten carbide ( $W_2C$ ) with hexagonal crystal structure. Moreover, it is also observed that the rGO reinforced WC-25 wt% Co coatings contain an additional phase of  $Co_3W_3C$  with face-centered crystal structure in addition to tungsten (W), tungsten carbide (WC), and semi-tungsten carbide ( $W_2C$ ) phases.

The tungsten (W) phase is not displayed here in the figures due to its very lesser intensity. The semi-tungsten carbide ( $W_2C$ ) phase is identified as a result of decarburization of WC at higher temperatures during the deposition of coatings. The  $W_2C$  phase is identified in WC grains and exhibits a fully shell type structure along with the boundaries of WC particles. The  $Co_3W_3C$  phase was allocated above the WC-Co splats [31]. During solidification process the  $Co_3W_3C$  phase is often identified in crystal forms. It is evident from earlier works that the wear characteristics of the coatings depend on the shape, size and also allocation of  $Co_3W_3C$  phase. The smaller amount of  $Co_3W_3C$  phase outcomes in superior wear resistance of coatings [32]. It can be noted that the phases present in 0.5, 1, and 1.5 wt% rGOs reinforced coatings the phases present are same, and hence the XRD patterns were revealed only for the 1.5 wt% rGOs reinforced coatings (see Fig. 8b). It can also be observed that the intensity of the cobalt phase is very minimal in coatings obtained at higher percentage of the rGOs addition, i.e., the cobalt phase is identified with higher intensity only in the case of 1.5 wt% rGOs added coating system.

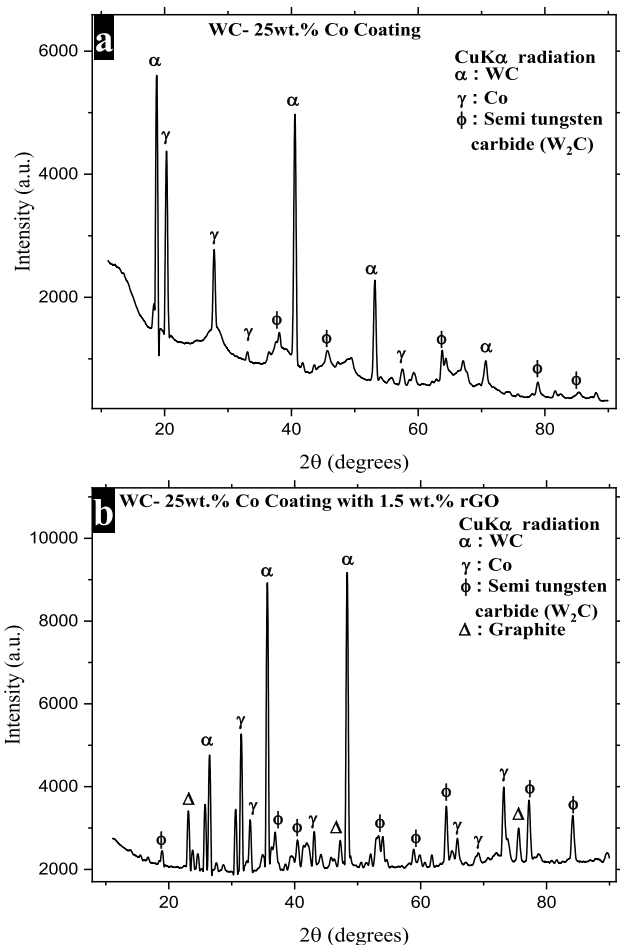


**Fig. 8** Phase analysis of WC-25 wt% Co coatings **a** without rGO, **b** with 1.5 wt% rGO

### 3.2 Mechanical properties

The microhardness of WC-25 wt% Co coatings gained from rGOs reinforced feedstock powder is evaluated and the variation in microhardness is shown in Fig. 9. It is noted that the microhardness of the coatings without adding the rGOs is  $10.8 \pm 0.11$  GPa, whereas with the addition of 1.5 wt% rGO, microhardness is obtained as  $12.1 \pm 0.15$  GPa. It can be observed that there is an increment in the microhardness of coatings with the addition of rGO. From the results, it is evident that the microhardness of coatings increases somewhat with raise in the rGO percentage addition (see Fig. 9). This phenomenon was occurred mainly because of rGO bridges obtained in the coating microstructure, and similar result was also identified in the work done by Jambagi et al., 2018, where CNTs (carbon nanotubes) were used instead of rGO [33]. However, there is no much significant variation in the microhardness as the difference in percentage

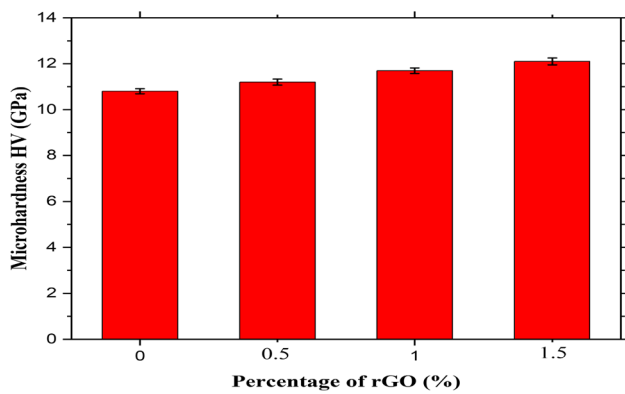


**Fig. 9** Variation in microhardness of WC-25 wt% Co coatings with variation in rGO percentage

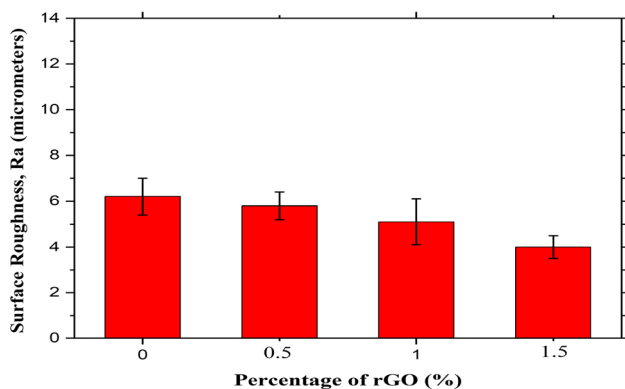


**Fig. 10** Variation in surface roughness of WC-25 wt% Co coatings with variation in rGO percentage

addition of rGO is very less (i.e., 0.5, 1.0, and 1.5 wt%). It can also be noticed that the microhardness of coatings is gradually increasing with the increased percentage of rGOs addition. This is on predictable lines that as the rGO percentage increases, the porosity in coatings reduces, and thus hardness increases [34].

The surface roughness of the as-sprayed coatings gained with and without addition of rGOs has been measured and shown in Fig. 10. It could be identified from Fig. 10 that the average surface roughness (Ra) of the as-sprayed coatings has been reducing with the raising the percentage of rGOs. The maximum values of average surface roughness obtained for the WC-25 wt% Co coatings with and without addition of rGOs are  $4.0 \pm 0.5 \mu\text{m}$  and  $3.6 \pm 0.3 \mu\text{m}$ , respectively. It is also observed physically through keen visual examination that the coatings obtained without the rGOs reinforcement are rough as compared to the coatings

obtained with the rGOs reinforcement. The main reason for this occurrence is that the nanostructured WC-25 wt% Co coatings without addition of rGOs exhibit more pores and show higher surface roughness, whereas the coatings reinforced with rGO have less pores and hence the as-sprayed coating's surface becomes smooth. The surface roughness values are recorded low for the rGO added coatings as compared to the coatings without the addition of rGO. When the rGOs are added, the pores get decreased in the nanostructured WC-25 wt% Co coatings as the rGOs are behaving nano type fillers and packing the void spaces of pores, and thus resulting in the smooth coating surface with reduced porosity [35].

### 3.3 Wear characteristics

Tribological types tests are performed on the as-sprayed coatings and wear behavior have been studied. From wear tests results, it was identified that the WC-25 wt% Co coatings with 1.5 wt% rGO shown less weight loss and a lesser amount of wear rate with lessen coefficient of friction as compared to the WC-25 wt% Co coatings with 0.5 wt% rGO and 1.0 wt% rGO [36]. The sum of weight loss goes after a critical trend at all the test parameter situations. The variation in weight loss at various loads and sliding speeds is displayed in Fig. 11. It could be observed that the sum of weight reduction (i.e., weight loss) is a smaller amount for the coatings obtained from 1.5 wt% rGO addition at all the sliding speeds of 0.16 m/s, 0.31 m/s, and 0.47 m/s. However, the weight loss followed a various trend in the coatings gained from 1.0 wt% rGOs addition at the sliding speed of 0.31 m/s. First, the weight loss increased up to 1 kgf load and then decreased (see Fig. 11b). This occurrence was mainly because of more decarbonization that happened at the time of coatings deposition. It can be understood that the decarbonization resulted in more softening of the coatings due to loss of carbon and hence more weight loss is occurring particularly at higher loads.

However, at the sliding speed of 0.16 m/s, the weight loss was noted a lesser amount as compared to the other two different types of sliding speeds. This observable fact can be accredited to the existence of an affluent protective layer created by rGO.

Also, the results are attained for the duration of wear tests for coefficient of friction (COF), wear rate, and wear depth at various test factor conditions. The difference in average coefficient of friction (COF) adjacent to normal load at various sliding speeds is shown in Fig. 12. It can be

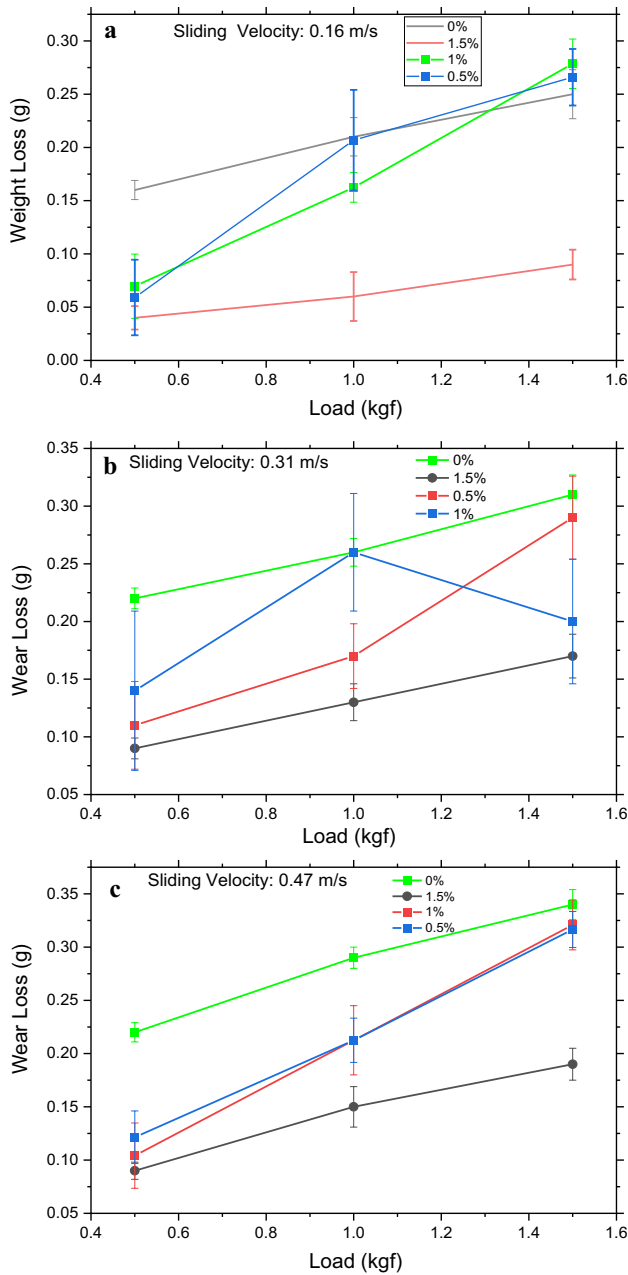


**Fig. 11** Weight loss as a function of normal load for WC-25 wt% Co coatings with 0 wt%, 0.5 wt%, 1.0 wt% and 1.5 wt% rGOs at a sliding speed of **a** 0.16 m/s, **b** 0.31 m/s and **c** 0.47 m/s

identified that the lesser value of COF is  $0.19 \pm 0.01$  and it is obtained for the coatings with 1.5 wt% rGOs addition at 1.5 kgf load and 0.16 m/s sliding speed. For these coatings, the wear rate is exceptionally low and the rGO would not be dragged out from coatings. Hence, the unspooled rGOs behave like protecting layers and present a low COF

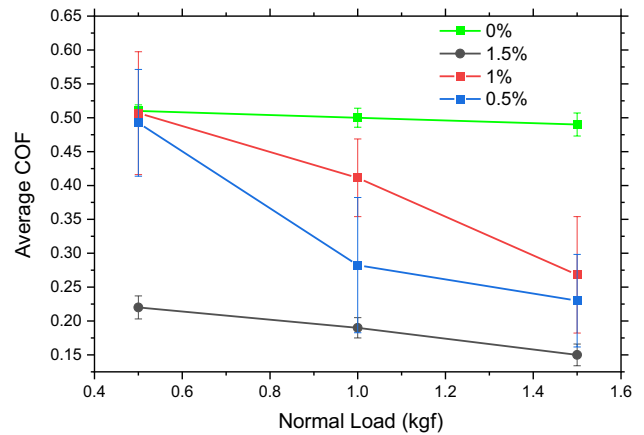


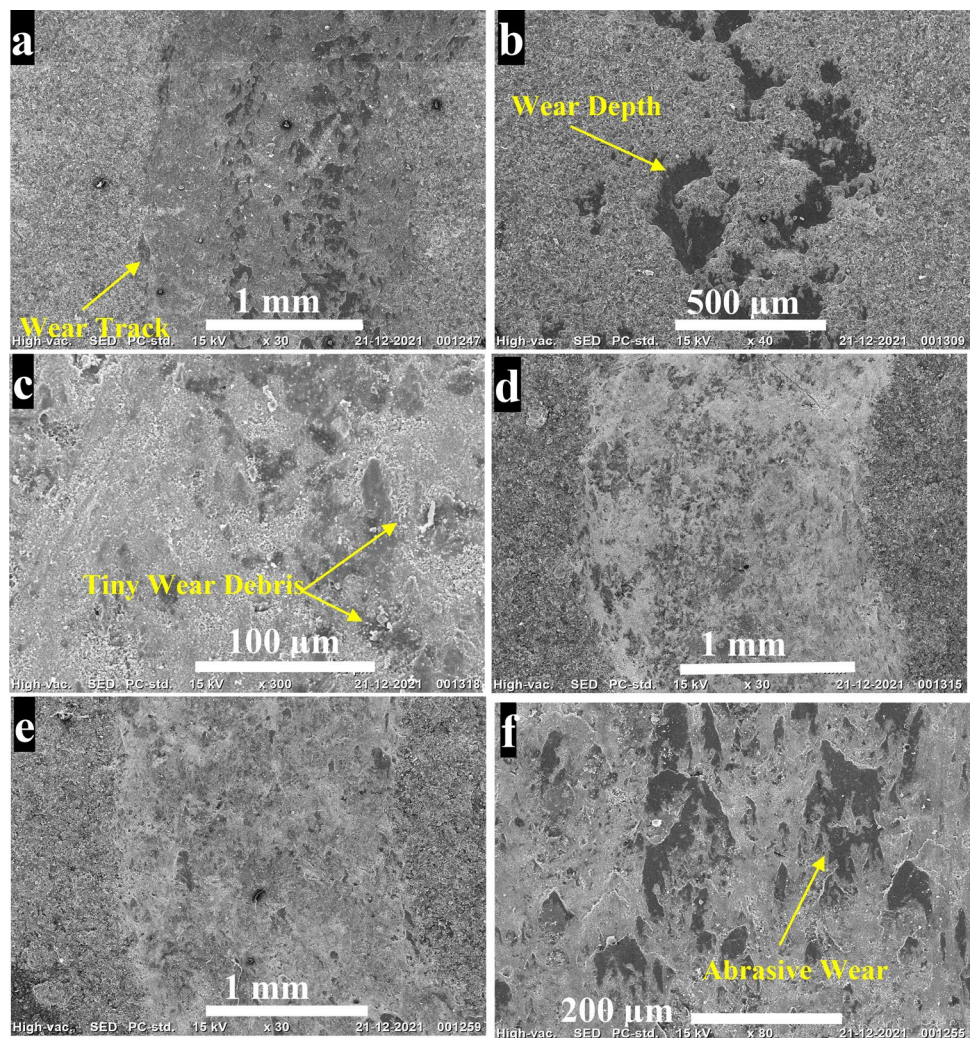
**Fig. 12** Average COF vs normal load for WC-25 wt% Co coatings reinforced with 0 wt%, 0.5 wt%, 1.0 wt%, and 1.5 wt% rGOs. at a sliding speed of 0.16 m/s, 0.31 m/s, and 0.47 m/s

[26]. It can be noted from Fig. 10 that the COF decreases with rGOs percentage rising. The existence of rGOs in WC-25 wt% Co coatings behaves like bridges with the aim of protect the coatings surface. This same identification was also examined in earlier studies as mentioned here [37–40].

The coatings morphology of wear track obtained from WC-25 wt% Co powders with rGOs reinforcement at load of 1.5 kgf and sliding speed of 0.17 m/s is exhibited in Fig. 13. It can be identified that the 0.5 wt% rGO added sample top coat has gone through delimitation (see Fig. 13a) caused by WC ball abrasive behavior over the surface of coating and the wear rate of this coating top coat exhibited maximum with higher wear depth as a result of rGO existence in lower weight percentage (see Fig. 13b). Besides, the coatings resulting from 1 wt% added rGOs are exhibiting similar type of delimitation phenomena but with lower intensity as evaluated to the 1.5 wt% of rGOs added coatings (see Fig. 13c). It can also be confirmed from the wear track morphology shown in Fig. 13d. The wear track morphology showed rough texture behavior because of high load. It can be noted that the coatings obtained from 1.5 wt% addition of rGOs, the deflection of cracks observed, it is due to existence of rGOs (see Fig. 13e) and this happened mainly because of rGOs induced type crack arresting method. Correspondingly, in 1.5 wt% rGOs added coatings, the surface of coating exhibits numerous patches that perform as protection layers and decreases the COF. These dark type patchy layers form mainly because of rGOs bridge formation in splats. The wear debris stripping on the surface of wear track can be mainly accredited to unspooled rGOs presence



**Fig. 13** Wear track morphology for coatings obtained from tungsten carbide–cobalt powders at different magnifications **a, b** coatings deposited with 0.5 wt% rGO, **c, d** coatings deposited with 1.0 wt.% rGO and **e, f** coatings deposited with 1.5 wt% rGO. Micrographs shown were for a normal load of 1.5 kgf, sliding speed of 0.17 m/s and sliding distance of 300 m



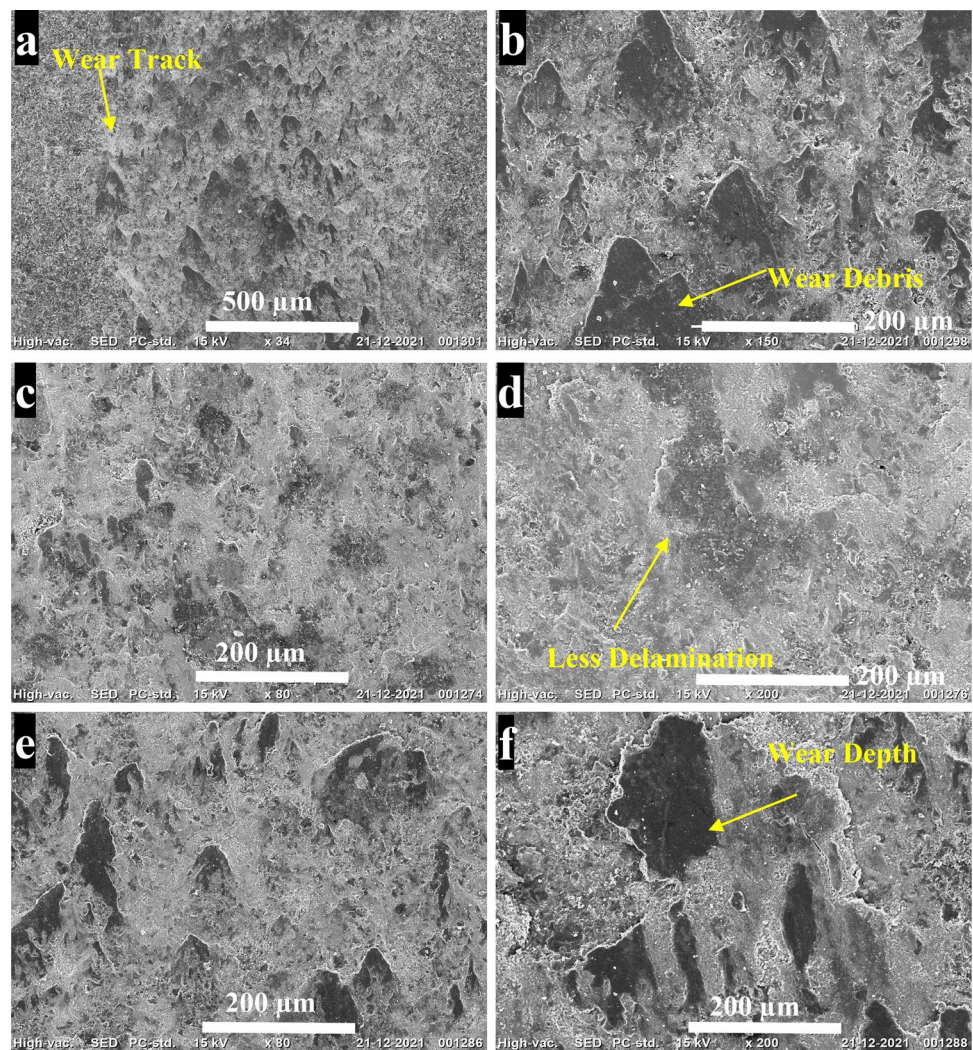
in coating microstructure (observe Fig. 13f). Nevertheless, it can be evidently noted that the wear of 0.5 wt% and 1.0 wt% rGOs added coatings occurred primarily because of delamination subsequently pulverization, while in 1.5 wt% of rGOs-added coatings, the sliding abrasive wear is identified, that is more dominant type of key wear mechanism.

Correspondingly, the wear track morphologies acquired for two types of sets with other conditions are also revealed in Figs. 14 and 15. The wear tracks obtained at load of 1.0 kgf, sliding speed of 0.33 m/s, and load of 0.5 kgf, sliding speed of 0.17 m/s test situations have been investigated, as shown in Figs. 14 and 15, correspondingly. At load of 1.0 kgf and sliding speed of 0.5 m/s condition, the wear tracks can be identified evidently in all type of coatings performed at various proportions of rGOs. It is identified in the coatings with 0.5 wt.% rGOs

in addition, the grooves and cracks were observed on wear tracks and tiny debris presence also noted on surface of the coating (see Fig. 14a, b). In the case of 1.0 wt% rGO added coatings, the discontinuous manner wear track was identified, it is because of brittle phases presence (see Fig. 14c, d). The reason for grooves observed on the surface of wear track is due to WC ball fluctuation at the time of wear test (see Fig. 14e). The wear fragments and micro-cracks initiation also can be observed on surface of the 1.5 wt% rGOs added coatings (see Fig. 14f). This occurred importantly because of the increasing of rGO weight percentage. In addition pulverized debris identified that indicates the existence of abrasive wear (see Fig. 14e). Nevertheless, it can be proved that there is not a lot change noticed in wear mechanism at these test conditions is primarily as a result of particles ablation of coated surface.



**Fig. 14** Wear track morphology for tungsten carbide–cobalt coatings at different magnifications **a, b** coatings deposited with 0.5 wt% rGO, **c, d** coatings deposited with 1.0 wt% rGO and **e, f** coatings deposited with 1.5 wt% rGO. Results shown were for a normal load of 1.0 kgf, sliding speed of 0.33 m/s and sliding distance of 300 m



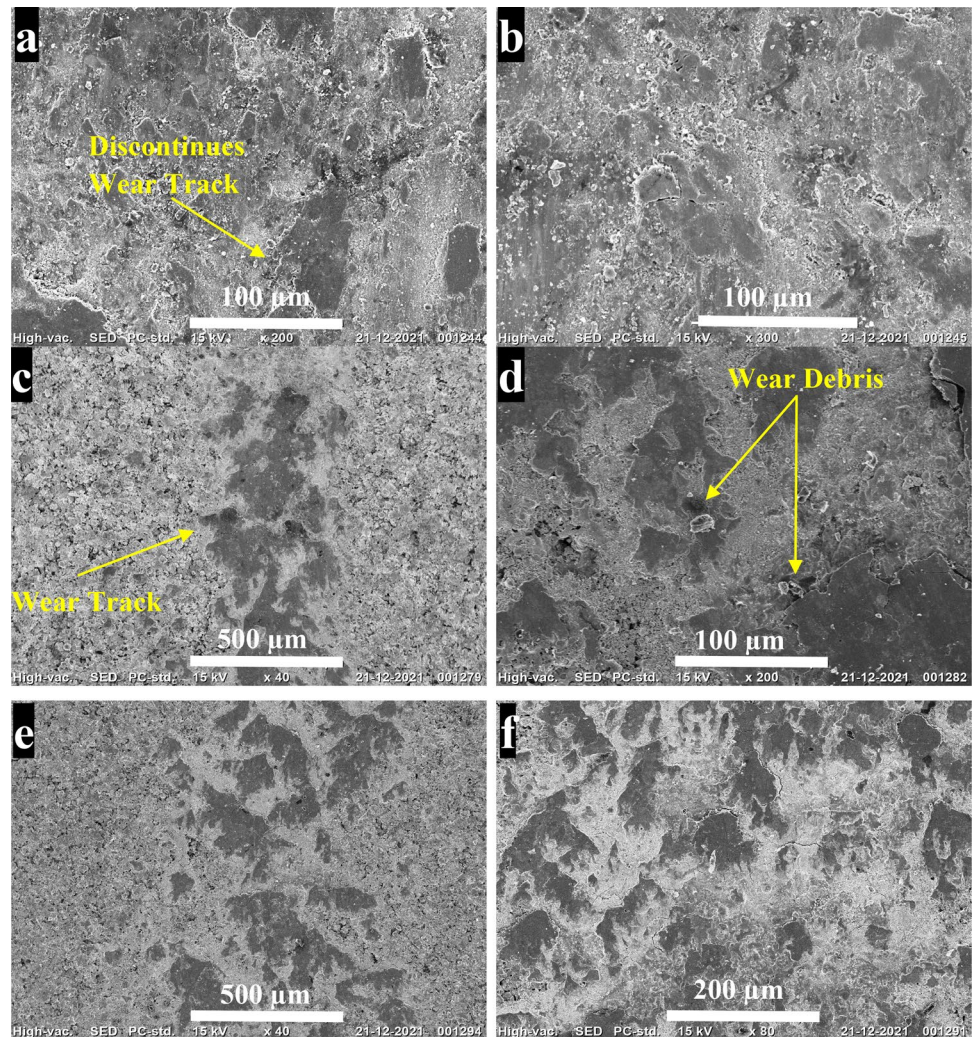
The wear track morphology attained at load of 0.5 kgf and sliding speed of 0.5 m/s on the worn-out surface for the coatings resulting from 0.5, 1, and 1.5 wt% rGO addition is noticed in Fig. 15. It was observed that for these loading conditions, the wear tracks were not produced clearly and discontinuous, but the wear loss was maximum with slightly higher wear depth (see Fig. 15a). It can also notice that at loading condition of 0.5 kgf, the wear depth is increasing drastically (see Fig. 15b). In addition the coatings gained from 1.0 wt% rGO addition, tiny wear debris identified because of fluctuations in loading. It can be seen that pulverized regions and rGOs bridges are existed throughout the coating splats (see Fig. 15c, d). Nevertheless, it can be identified that the wear tracks are in smooth texture. From Fig. 15e, f, it can also be noted that the coatings performed from 1.5 wt% rGOs addition, at higher magnification wear track was extremely slight even and the rGO particles adhered on the wear track.

## 4 Conclusions

The WC-25 wt% Co nanostructured coatings added with 0.5, 1, and 1.5 wt% rGOs were obtained by HVOF spraying. The rGOs were present in the coatings even after spraying them at elevated temperatures. A major improvement was observed in the microhardness and surface roughness with rGOs reinforcement in the nanostructured coatings. Microstructural characteristics of the coatings were also changed, and the rGO bridges among the splats were observed in the coating's microstructure. For 1.5 wt% rGO added coatings, the wear rate was extremely low and the rGO could not be taken out from the coatings. Later, the unpulled rGOs acted as protective layers and offered a low coefficient of friction. It was identified that the wear occurred in 0.5 wt% of rGOs and 1.0 wt% rGOs added coatings was mostly because of delimitation followed by pulverization specifically at 1.5 kgf



**Fig. 15** Wear track morphology for tungsten carbide–cobalt coatings at different magnifications **a, b** coatings deposited with 0.5 wt% rGO, **c, d** coatings deposited with 1.0 wt% rGO and **e, f** coatings deposited with 1.5 wt% rGO. Results shown were for a normal load of 0.5 kgf, sliding speed of 0.5 m/s and sliding distance of 300 m



load and 0.17 m/s sliding speed, while the sliding abrasive wear phenomenon was the most dominant primary wear mechanism in the case of 1.5 wt% rGOs added coatings. Hence, this study helps to reduce the wear rate effectively in various industrial applications especially, for nozzles, turbine blades, automotive spare parts, etc.

**Acknowledgements** Dr. B. Venkateshwarlu and A. Srikanth acknowledge the Science and Engineering Research Board (SERB), Department of Science and Technology (DST), New Delhi, India for providing the financial support to this research work via Project No.: EEQ/2017/000096.

**Data availability** The authors confirm that the data supporting the findings of this study are available within the article and its Supplementary material. Raw data that support the findings of this study are available from the corresponding author, upon reasonable request.

## Declarations

**Conflict of interest** The authors declare that they have no known competing financial interests or personal relationships that could have appeared to influence the work reported in this paper.

## References

1. Author, *Mater. Sci.* **14**, 345 (2008).
2. S. Das, T.K. Bandyopadhyay, S. Ghosh, A.B. Chattopadhyay, P.P. Bandyopadhyay, *Metall. Mater. Trans. A* **34**, 1909 (2003)
3. H. Liang, B. Shi, A. Fairchild, T. Cale, *Vacuum* **73**, 317 (2004)
4. H. Chen, S. Lee, X. Zheng, C. Ding, *Wear* **260**, 1053 (2006)
5. B. Liang, H. Liao, C. Ding, C. Coddet, *Thin Solid Films* **484**, 225 (2005)
6. S. Guessasma, M. Bounazef, P. Nardin, T. Sahraoui, *Ceram. Int.* **32**, 13 (2006)
7. P.P. Psyllaki, M. Jeandin, D.I. Pantelis, *Mater. Lett.* **47**, 77 (2001)
8. N. Vaxevanidis, D. Manolacos, G.P. Petropoulos, *Tribol. Ind.* **26**, 42 (2004)
9. J.H. Ouyang, S. Sasaki, *Ceram. Int.* **27**, 251 (2001)
10. A.A.E. Hassan, N.H. Menzler, G. Blass, M.E. Ali, H.P. Buchkremer, D. Stöver, *J. Mater. Sci.* **37**, 3467 (2002)
11. D.D. Green, P.A. Williams, G. Pezzotti, I.C. Clarke, *Key Eng. Mater.* **240–242**, 827 (2003)

12. K.S. Novoselov, A.K. Geim, S.V. Morozov, D. Jiang, M.I. Katsnelson, I.V. Grigorieva, S.V. Dubonos, A.A. Firsov, *Nature* **438**, 197 (2005)
13. A. Srikanth, V. Bolleddu, *J. Therm. Spray Technol.* (2023). <https://doi.org/10.1007/s11666-023-01556-8>
14. A.T. Dideikin, A.Y. Vul', *Front. Phys.* (2019). <https://doi.org/10.3389/fphy.2018.00149>
15. D.G. Trikkaliotis, A.K. Christoforidis, A.C. Mitropoulos, G.Z. Kyzas, *ChemEngineering* **5**, 64 (2021)
16. C. Gómez-Navarro, M. Burghard, K. Kern, *Nano Lett.* **8**, 2045 (2008)
17. C. Lee, X. Wei, J.W. Kysar, J. Hone, *Science* **321**, 385 (2008)
18. Md.S. Islam, Y. Shudo, S. Hayami, *Bull. Chem. Soc. Jpn.* **95**, 1 (2022)
19. J.A. Buledi, N. Mahar, A. Mallah, A.R. Solangi, I.M. Palabiyik, N. Qambrani, F. Karimi, Y. Vasseghian, H. Karimi-Maleh, *Food Chem. Toxicol.* **161**, 112843 (2022)
20. J.S. Bunch, S.S. Verbridge, J.S. Alden, A.M. van der Zande, J.M. Parpia, H.G. Craighead, P.L. McEuen, *Nano Lett.* **8**, 2458 (2008)
21. G. Chen, W. Weng, D. Wu, C. Wu, J. Lu, P. Wang, X. Chen, *Carbon* **42**, 753 (2004)
22. J. Campos-Delgado, Y.A. Kim, T. Hayashi, A. Morelos-Gómez, M. Hofmann, H. Muramatsu, M. Endo, H. Terrones, R.D. Shull, M.S. Dresselhaus, M. Terrones, *Chem. Phys. Lett.* **469**, 177 (2009)
23. F.L. Zhang, C.Y. Wang, M. Zhu, *Scr. Mater.* **49**, 1123 (2003)
24. A.H. Dent, S. DePalo, S. Sampath, *J. Therm. Spray Technol.* **11**, 551 (2002)
25. F. Ghadami, S. Ghadami, H. Abdollah-Pour, *Vacuum* **94**, 64 (2013)
26. P.K. Aw, A.L.K. Tan, T.P. Tan, J. Qiu, *Thin Solid Films* **516**, 5710 (2008)
27. G.M.T. Basha, B. Venkateshwarlu, *I.O.P. Conf. Ser. Mater. Sci. Eng.* **1123**, 012065 (2021)
28. A. Nieto, D. Lahiri, A. Agarwal, *Carbon* **50**, 4068 (2012)
29. I. Ahmad, M. Islam, T. Subhani, Y. Zhu, *J. Mater. Eng. Perform.* **24**, 4236 (2015)
30. B. Mukherjee, O.S. Asiq Rahman, A. Islam, M. Sribalaji, A.K. Keshri, *J. Alloys Compd.* **727**, 658 (2017)
31. J. Yuan, Q. Zhan, J. Huang, S. Ding, H. Li, *Mater. Chem. Phys.* **142**, 165 (2013)
32. A. Formisano, F. Capece Minutolo, A. Caraviello, L. Carrino, M. Durante, A. Langella, *Adv. Tribol.* **2016**, e5063274 (2016)
33. S.C. Jambagi, A. Agarwal, N. Sarkar, P.P. Bandyopadhyay, *J. Mater. Eng. Perform.* **27**, 2364 (2018)
34. X.-T. Luo, C.-X. Li, F.-L. Shang, G.-J. Yang, Y.-Y. Wang, C.-J. Li, *J. Therm. Spray Technol.* **24**, 100 (2015)
35. S. Priyadershini, O.S.A. Rahman, K.K. Pandey, A.K. Keshri, *Ceram. Int.* **45**, 5768 (2019)
36. H. Myalska, G. Moskal, K. Szymański, *Surf. Coat. Technol.* **260**, 303 (2014)
37. K. Goyal, H. S. Sidhu, R. Bhatia, *Int. J. Mech. Eng. Robot. (IJMER)*. **3**, 2321–5747 (2015)
38. M. Heydarzadeh Sohi, F. Ghadami, *Tribol. Int.* **43**, 882 (2010)
39. S. Ariharan, A. Nisar, N. Balaji, S.T. Aruna, K. Balani, *Compos. Part B Eng.* **124**, 76 (2017)
40. K. Goyal, H. Singh, R. Bhatia, *J. Aust. Ceram. Soc.* **55**, 315 (2019)

**Publisher's Note** Springer Nature remains neutral with regard to jurisdictional claims in published maps and institutional affiliations.

Springer Nature or its licensor (e.g. a society or other partner) holds exclusive rights to this article under a publishing agreement with the author(s) or other rightsholder(s); author self-archiving of the accepted manuscript version of this article is solely governed by the terms of such publishing agreement and applicable law.